PHASE TRANSITIONS IN ANTIFERROMAGNETS IN EXTERNAL MAGNETIC FIELDS: MÖSSBAUER SPECTROSCOPY

R. B. Frankel
Francis Bitter National Magnet Laboratory*
Massachusetts Institute of Technology
Cambridge, Massachusetts 02139

I. INTRODUCTION

Known antiferromagnetic materials far out number known ferromagnetic and ferrimagnetic materials. Moreover, the antiferromagnets display a wide variety of phase transitions in addition to the paramagnetic to antiferromagnetic transition at the Néel point, that make them a rich source of information about the relationship between exchange interactions, structure, and phase transition phenomena. Mössbauer spectroscopy has been used extensively over the last decade to study antiferromagnets, capitalizing on the fact that the magnetic hyperfine field is proportional to the sublattice magnetization. In general, these studies have concentrated on determining the magnetic structure below T_N and the sublattice magnetization as a function of T below T_N, in some cases in the critical region. Less well studied are those transitions in antiferromagnets which are induced by external magnetic fields, although in these cases too, Mössbauer spectroscopy can provide important and often unique information.

In this paper we will review some applications of Mössbauer spectroscopy to the study of phase transitions in antiferromagnets induced by external magnetic fields. In Sec. II below we will briefly recapitulate the molecular field approximation (MFA) and review the phase transitions in antiferromagnets; in Sec. III we will make some general

remarks about Mössbauer spectroscopy of these transitions; in Sec. IV we will briefly review some applications to specific materials.

II. PHASE TRANSITIONS IN SIMPLE UNIAXIAL ANTIFERROMAGNETS

A. Phases and Phase Boundaries [1-5]

The simplest kind of antiferromagnet consists of two interpenetrating sublattices, 1 and 2, where the spin moment of a magnetic ion at any given site is antiferromagnetically coupled to the spin moments of its neighboring ions. Thus at temperatures below T_N and external magnetic field $H_o = 0$, the sublattice moments, σ_1 and σ_2 are antiparallel to each other. The orientation of σ_1 and σ_2 relative to the crystal structure of the material is determined by the so-called anisotropy energy. If the anisotropy energy has uniaxial symmetry and is of such magnitude and sign such that the axis of symmetry (say the a-axis) is the preferred direction of σ_1 and σ_2, then the antiferromagnet is called uniaxial and of the easy-axis type.

Below T_N, a critical value of an external magnetic field $H_o = H_{SF}$ applied parallel to the a-axis will induce a first-order-phase transition to a phase in which σ_1 and σ_2 are roughly perpendicular to each other and perpendicular to the a-axis (in the basal plane). This phase is known as the spin-flop phase (SF). If H_o is increased beyond H_{SF} then σ_1 and σ_2 tip toward each other and the a-axis until a second critical value of the external field $H_o = H_P$ induces a second-order-phase transition to the paramagnetic phase (P) in which σ_1 and σ_2 are parallel to each other and parallel to the a-axis.

Both H_{SF} and H_P are determined by the exchange energy and the anisotropy energy (see below), and as both are temperature dependent, the critical magnetic fields H_{SF} and H_P are also temperature dependent, and a representative phase diagram of a uniaxial, easy-axis antiferromagnet is shown in Fig. 1a. There is a triple point (H_3, T_3) where all three phases coexist; for $T > T_3$, only the AF and P phases exist.

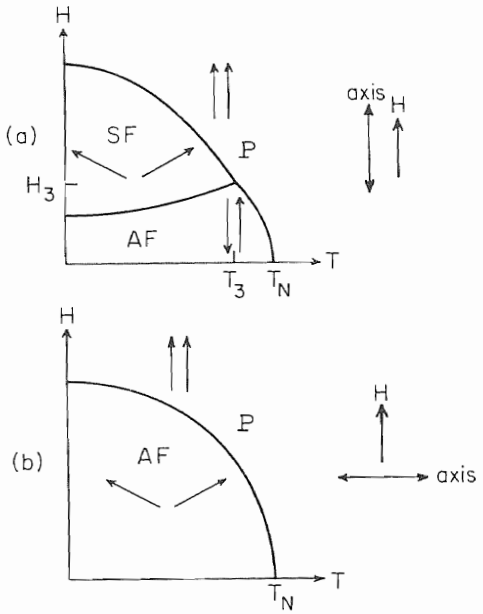

Fig. 1. Schematic phase diagram for uniaxial, easy-axis antiferromagnet: a) H_o parallel to the easy axis; b) H_o perpendicular to the easy axis (after Ref. 2).

A magnetic field applied perpendicular to the easy axis for $T < T_N$ will induce a phase transition from the AF phase to the P phase, as shown in Fig. 1b. In this case, the field causes the spins to tip toward each other and away from the a-axis until the critical field H_{AFP} causes the transition to the P phase, where they are parallel to each other and perpendicular to the a-axis. There is no SF phase for the orientation of H_o relative to the a-axis.

B. Thermodynamics of the Spin Flop

The spin-flop transition is of first-order thermodynamically and can be understood as follows.[5] As the analog of the Gibbs potential for nonmagnetic systems, we define $\Phi(T, P, H)$, the thermodynamic potential for the antiferromagnet. The equilibrium configuration of spins is that configuration for which $\Phi(T, P, H)$ is a minimum. At constant T and P,

$$\Phi(H) = \Phi(0) - \frac{1}{2} \chi H_o^2 \tag{1}$$

where χ is the magnetic susceptibility. At $H = 0$, $\Phi_{AF}(0) < \Phi_{SF}(0)$ and

$$\Phi_{SF}(0) = \Phi_{AF}(0) + K, \tag{2}$$

where K is the anisotropy energy. The critical field H_{SF} is by definition that field for which the AF and SF phases coexist, or

$$\Phi_{AF}(H_{SF}) = \Phi_{SF}(H_{SF}). \tag{3}$$

Using Eqs. (1) and (2), Eq. (3) leads to

$$H_{SF} = \left[\frac{2K}{\chi_{SF} - \chi_{AF}} \right]^{1/2} \tag{4}$$

Since $\chi_{AF} = \chi_{\parallel}$, the low field susceptibility with H_o oriented along the a-axis, and $\chi_{SF} \simeq \chi_{\perp}$, the low field susceptibility with H_o oriented perpendicular to the a-axis, Eq. (4) can be rewritten as

$$H_{SF} = \left[\frac{2K}{\chi_{\perp} - \chi_{\parallel}} \right]^{1/2} . \qquad (5)$$

$\chi_{\parallel}$ approaches zero at T goes to zero while $\chi_{\perp}$ is roughly constant below T_N for an ideal, uniaxial antiferromagnet (see Fig.2). Above T_N $\chi_{\parallel} \approx \chi_{\perp}$. Moreover, $\chi_{\perp} - \chi_{\parallel}$ usually decreases faster than K so that H_{SF} increases with increasing T.

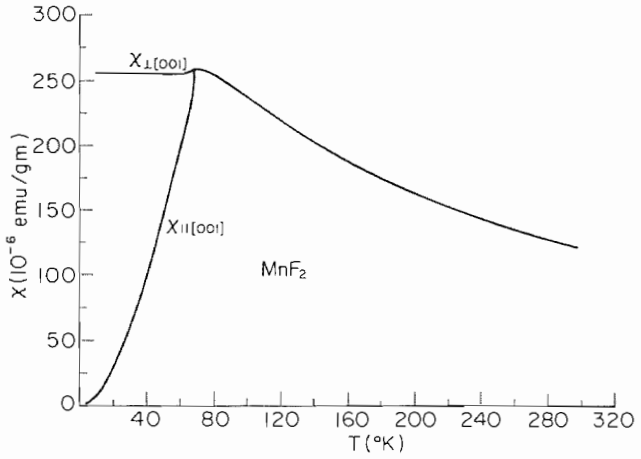

Fig. 2. $\chi_{\parallel}$ and $\chi_{\perp}$ plotted as a function of temperature for the ideal uniaxial antiferromagnet MnF_2 (after Ref. 1).

C. Molecular Field Approximation

If we assume that the ions on one sublattice interact only with the neighboring ions on the other sublattice, then the molecular field approximation (MFA) consists in replacing the exchange interaction by an effective exchange field which is proportional to the magnetization of the other sublattice. If the spin of the transition metal ion is S, then the magnetization $\sigma = \langle S \rangle / S$ is given by a Brillouin function

$$\sigma_1 = B_s \left[\frac{g\mu_B S H_1}{kT} \right], \tag{6}$$

where H_1 is the total field given by

$$H_1 = H_o + H_{ex} = H_o - \lambda \sigma_2. \tag{7}$$

The expressions for σ_2 are similar. The constant λ includes the number of neighbors and the exchange integral.[2, 3, 4]

In the MFA, the AF to P phase boundary is given by[2]

$$H_{AFP} = 2\lambda\sigma(T) \tag{8}$$

where $\sigma(T)$ is calculated with $H_o = 0$. Close to T_N, this leads to an expression of the form[2, 4]

$$T_N - T = D\, H_{AFP}^2, \tag{9}$$

where D is a constant, i.e., that the depression of the Néel point is quadratic in magnetic field. For $H_o \perp a$, the phase boundary has the same form, with $D(H_o \perp a) \approx 1/3\, (D(H_o \parallel a)$.[2]

The MFA predicts a similar form for the SF to P phase boundary, except that small corrections for the anisotropy energy must be included, which change the extrapolated zero field transition temperature from T_N. More sophisticated calculations predict

$$H_P(T) = H_P(0) \left[1 - aT^{3/2} \right], \tag{10}$$

for $T \rightarrow 0$, where a is a constant.

The MFA can also be used to calculate the individual sublattice magnetizations for $H_o \parallel a$ and $T_3 < T \leq T_N$ and $T > T_N$.[2, 4] Although $\sigma_1 = -\sigma_2$ for all T when $H_o = 0$, in finite H_o this is no longer the case. Moreover $\sigma_1 = \sigma_2 \neq 0$ for $T > T_N$ if $H_o \neq 0$, but $\sigma_1 \neq -\sigma_2$ for $T < T_N$. The expected sublattice magnetizations as a function of H_o are indicated schematically in Fig. 3. The sublattice magnetizations as function of T at constant H_o have a similar form.

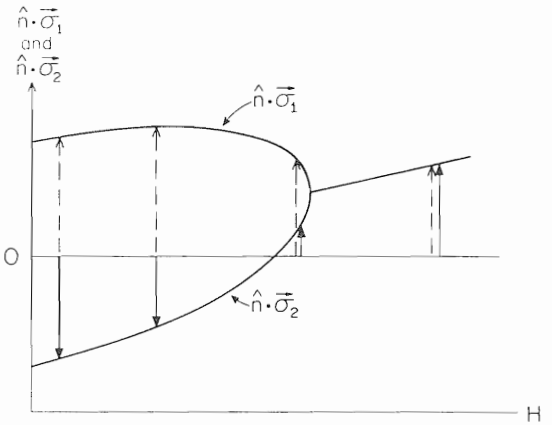

Fig. 3. Magnetic field dependence of $\hat{n}\cdot\vec{\sigma}_1$ and $\hat{n}\cdot\vec{\sigma}_2$ at constant T, $T_3 < T < T_N$. $\hat{n}$ is a unit vector pointing parallel to $\vec{H}_o$ and along the easy axis. The solid and dashed arrows represent $\vec{\sigma}_1$ and $\vec{\sigma}_2$, respectively (after Ref. 2).

It is well known that the MFA breaks down in the critical region, i.e., close to T_N. Here it is more appropriate to use this expression

$$\sigma_i = A(1 - T/T_N)^{\beta}, \qquad (11)$$

where A is a constant and β is a constant, usually 0.33 for a three-dimensional antiferromagnet. This expression is also suitable for measurements in external magnetic fields, as is shown below in Sec. IV-A. In external fields however, one uses

$$\vec{L} = \frac{\vec{\sigma}_1 - \vec{\sigma}_2}{2},$$

to compare with the second member of Eq. (11).

Since the magnitude of H_{SF} depends on the anisotropy energy (Eq. (5)), the spin-flop transition will be observable with available fields only for those materials for which this energy is relatively small. It can be shown that $\chi_{\perp} \simeq 1/\lambda$ and taking $\chi_{\parallel}/\chi_{\perp} \approx \delta$, Eq. (5) can be written[1]

$$H_{SF} = \left[\frac{2\lambda K}{1 - \delta}\right]^{1/2} . \qquad (12)$$

If we write the anisotropy energy K in terms of an anisotropy field $H_A = K/gS$, and remembering that the exchange field $H_E = \lambda gS$ in the MFA,

$$H_{SF} = \left[\frac{2H_E H_A}{1 - \delta}\right]^{1/2} . \qquad (13)$$

Since $\delta \approx 0$ at $T = 0$, it can be seen that for exchange fields of 10^6 Oe, the anisotropy field must be less than 10^4 Oe in order that the spin flop be observable in the laboratory ($H_o \approx 2 \times 10^5$ Oe).

D. More Complex Systems

Ideal situations are encounted infrequently in any area of experience, and so too with antiferromagnets. It would not be possible to recapitualte all the possible complications, however, one general type of transition should be mentioned. In the simple MFA above, we assumed that the entire exchange field acting on a given site was due to the neighboring ions on the other sublattice. An obvious extension of the model would be to include interactions of the ion with other ions on the same sublattice. In some cases the structure is such that the intra-sublattice interaction is stronger than the inter-sublattice interaction, i.e., the anisotropy field is effectively greater than the antiferromagnetic exchange field. If a field is applied along the easy axis, it may be possible to observe a first-order AF to P transition, called a metamagnetic transition. In certain cases, with more complex structures, intermediate ferrimagnetic phases can be observed with increasing H_o along a, all first-order thermodynamically.

III. HYPERFINE INTERACTIONS AND MÖSSBAUER SPECTROSCOPY

Associated with the phase boundaries outlined in the previous sections, there will be changes in the hyperfine spectrum which can be observed by Mössbauer spectroscopy. The general changes which one might observe are: a) the magnitude of the hyperfine interaction changes in going across the phase boundary with consequent shifts in the spectral lines; b) the polarization direction changes, with consequent changes in the relative intensities of the lines; c) the angle between the principle component of the electric field gradient and the magnetic hyperfine field changes with consequent shifts in the spectral lines.

Let us consider the expected changes with reference to a uniaxial antiferromagnet with H_o along the easy (a) axis (see Fig. 1a) and parallel to the γ-ray propagation direction. Let us further assume that V_{zz} is along a and $\eta = 0$. Then along the $H_o = 0$ line, above T_N one obtains a quadrupole spectrum only, while below T_N one obtains a single spectrum with the angle β between V_{zz} and $H_{hf} = 0$. Of course, $\vec{H}_{hf}$ is temperature dependent, going to zero at T_N. For a single crystal absorber, $\Delta m = 0$ lines have intensity zero.

A. AF Region

Since the total field at the nucleus is the sum of the hyperfine field and the applied field,

$$\vec{H}_n = \vec{H}_{hf} + \vec{H}_o, \qquad (14)$$

application of H_o along a results in two spectra, one in which $H_n = H_{hf} + H_o$, the other in which $H_n = H_{hf} - H_o$. Unless the sign of the hyperfine interaction is known (from measurements in the P phase, for example) it is not possible to say which spectrum corresponds to the spin up sublattice, and which corresponds to spin down. For both spectra, β remains zero and the intensity of the $\Delta m = 0$ lines equals 0. In crossing the AF-P phase boundary, H_{hf} will be proportional to σ and can be compared with the MFA calculations outlined above. Since both sublattices will, in general, have different magnetizations σ, so will the hyperfine fields for the ions on the two sublattices be different. In the

critical region it is appropriate to take the vector difference of the two hyperfine fields $\vec{H}_{hf}^{(1)} - \vec{H}_{hf}^{(2)}$ (not $\vec{H}_n^{(1)} - \vec{H}_n^{(2)}$) proportional to $\vec{L}$ to compare with Eq. (11).

B. SF Region

At $H_o = H_{SF}$, the two spectra collapse into a single spectrum with the $\Delta m = 0$ lines now the most intense. The angle β is now $\pi/2$, and $H_n \approx \sqrt{H_o^2 + H_{hf}^2}$. In addition, the magnitude (and possibly even the sign) of H_{hf} in the SF region, say H_{hf}^{SF}, may be different than in the AF region, say H_{hf}^{AF}. In Fe^{3+}, the change in H_{hf} is not expected to be large because Fe^{3+} is an S-state ion, but the change can be considerable in Fe^{2+} where the single ion anistropy can be large. If the spin-flop boundary is at large values of H_o, then the spins in the SF phase will be canted out of the basal plane toward a. This means that β will be less than $\pi/2$ and the appropriate vector sum of $\vec{H}_{hf}$ and $\vec{H}_o$ must be taken to give $\vec{H}_n$.

C. P Region

In the P region, after crossing either the SF-P phase boundary or the AF-P phase boundary, the spectrum is again a single spectrum with $H_n = H_{hf} \pm H_o$, depending on the sign of H_{hf}. Again, as in the AF region, $\beta = 0$ and the $\Delta m = 0$ lines have zero intensity. The magnitude of H_{hf} is H_o and T dependent, and the dependence can usually be approximated by a Brillouin function,

$$H_{hf} = H_{hf}^0 \, B_s \left(\frac{g\mu_B H_i}{kT} \right), \tag{15}$$

where H_{hf}^0 is the saturation value of the hyperfine interaction, i.e., the value of H_{hf} for $B_s = 1$, and H_i is the magnetic field acting on the ionic moment, including H_o and the exchange fields due to the other spins (Eq. (7) above).

D. H_o Applied Perpendicular to the a-axis

In this case we refer to the phase diagram in Fig. 1b. In the AF region, one now obtains a single spectrum for all

H_o with $H_n \approx \sqrt{H_o^2 + H_{hf}^2}$ and $\beta = 0$. If the γ-ray propagation direction is parallel to a, then the $\Delta m = 0$ lines will be absent. As H_o increases and the spins tip away from a, β will decrease and the $\Delta m = 0$ lines will increase in intensity. At the AF-P phase boundary H_{hf} and H_o are parallel, $\beta = \pi/2$ and the $\Delta m = 0$ lines have maximum intensity. The value of H_{hf} in the P phase may be different than that observed in the P phase with $H_o \parallel a$, reflecting anisotropy in the single ion properties.

IV. EXPERIMENTAL RESULTS

A. MnF_2

MnF_2 crystalizes in a rutile structure with a tetragonal lattice and two magnetic ions per unit cell. Below the Néel temperature $T_N = 67.4$ K, the magnetic properties of MnF_2 are understood in terms of an ideal, two sublattice, easy-axis antiferromagnet with the spins aligned along the c-axis. The phase diagram of MnF_2 has been studied by magnetic moment and ultrasonic techniques[2] and is shown in Fig. 4. H_{SF} is 93 kOe at 4.2 K; this low field is due to the fact that Mn^{2+} is an S-state ion and has low anisotropy.

Fe^{2+} may be isomorphously incorporated into the MnF_2 lattice, and zero field Mössbauer spectroscopy has been reported by Wertheim et al.[6] The addition of iron results in an increase of the Néel temperature and an increase in the value of H_{SF}, due to the fact that Fe^{2+} has a large single ion anistropy compared with Mn^{2+}. For 1% Fe in MnF_2, H_{SF} is 105 kOe.[7]

Spin Flop. The SF phase was observed by Abeledo et al.[8] using Mössbauer spectroscopy. A large single crystal of ~1% Fe^{2+} doped MnF_2 was grown from the melt by Optovac, Inc. The crystal was oriented and a 6 mil slice was taken perpendicular to the c-axis. H_o was applied parallel to the c-axis.

Spectra at 4.2 K and $H_o = 0$, 75 and 111 kOe are shown in Figs. 5a, 5b and 6 respectively. For $H_o = 0$ an apparent three line spectrum is observed, due to a fortuitous superposition of the inner $\Delta m = \pm 1$ lines. In the AF phase, $H_{hf}^{AF} = 227$ kOe, $\Delta E = 2.8$ mm/sec and $\beta = \pi/2$.[6] For $H_o < H_{SF}$, the spectrum (Fig. 5b) consists of the super-

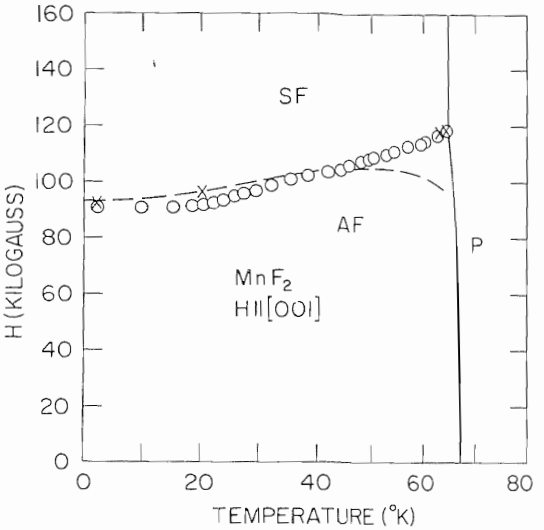

Fig. 4. AF-SF phase boundary in MnF_2, with H_o parallel to $[00\bar{1}]$ (after Ref. 2).

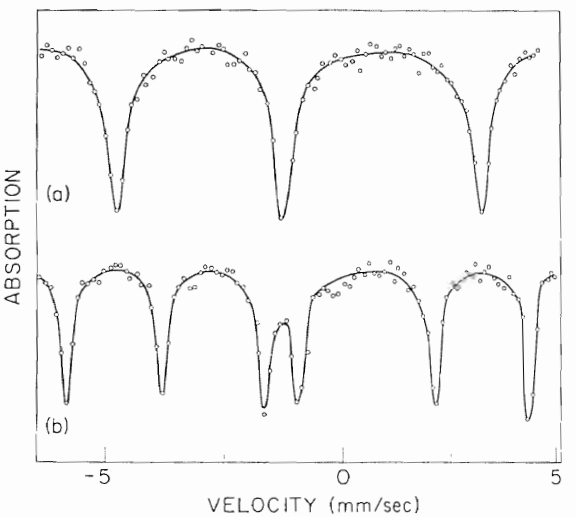

Fig. 5. Mössbauer spectra of single crystal $MnF_2:Fe^{2+}$: a) 4.2 K, $H_o = 0$; b) 4.2 K, $H_o = 75$ kOe; $\gamma \parallel H_o \parallel [00\bar{1}]$.

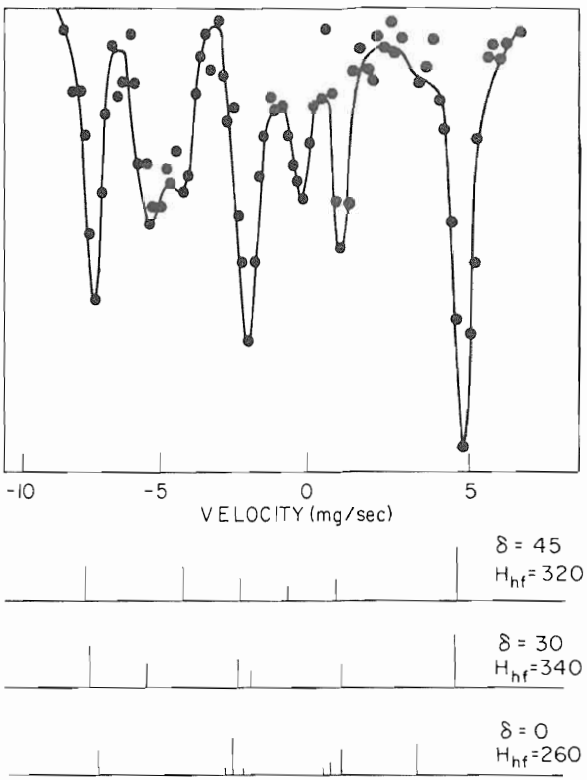

Fig. 6. Mössbauer spectrum of single crystal MnF_2 at 4.2 K, H_o = 111 kOe, in the SF phase. The bar diagrams below the figure represent the expected spectra for various orientations of the moment in the basal plane (after Ref. 8).

position of the two sublattice spectra as discussed in Sec.III.A. For $H_o > H_{SF}$, the spectrum (Fig. 6) changes dramatically due to the appearance of the $\Delta m = 0$ lines, and the field at the nucleus $\vec{H}_n = \vec{H}_o + \vec{H}_{hf}^{SF}$, where H_{hf}^{SF} is perpendicular to c. The spectrum is considerably complicated by the fact that there are two crystallographic sites for the transition metal ions with common c-axis but oriented at 90° with respect to each other in the basal plane, and each site has equivalent orthorhombic symmetry. V_{zz} is along [110] for one site and $[1\bar{1}0]$ for the other. If the spins flop to a [100] direction, β is the same for both sites. If spins flop to a [110] direction, $\beta = 0°$ for one site and 90° for the other, giving two superposed spectra. Moreover, since the site symmetry is orthorhombic, H_{hf}^{SF} is not the same for both sites, as the orbital contribution to the hyperfine interaction is anisotropic in the basal plane. Comparison of the observed spectrum with computer calculated spectra leads to a two domain model, in which one domain has spins oriented along [100], and the other has spins oriented (probably) along [110]. Hence there are three spectra with the following parameters: i) H_{hf}^{SF} ([100]) = ± 320 kOe, $\beta = 45°$, ii) H_{hf}^{SF} ([110]) = - 340 kOe, $\beta = 90°$, iii) H_{hf}^{SF} ([110]) = 260 kOe, $\beta = 0°$. These results have been analyzed to yield values of the g-factor of Fe^{2+} in the basal plane. For details see Ref. 8.

AF to P.[9] The phase diagram close to T_N is shown in Fig. 7. In Fig. 8 we show spectra for $H_o = 80$ kOe along the c-axis both above and below T_N. Below T_N the spectrum consists of eight lines, due to the superposition of two four-line spectra; above T_N the spectrum has collapsed to a single four-line spectrum. Since the field at the nucleus H_n is less than H_o, H_{hf}^P is negative. The field dependence of the phase boundary was determined by sweeping the temperature at constant field and the field at constant temperature, and is shown in Fig. 9, where H_o^2 at T_N is plotted as a function of T. The straight line corresponds to Eq. (9); also shown is corresponding phase boundary for pure MnF_2.[2]

In Fig. 10, the hyperfine field for each sublattice is shown plotted as a function of T for $H_o = 80$ kOe. The dashed line is the best fit with the MFA above and below T_N, and the solid line is the best fit with the MFA to the Néel point itself. In this case the MFA is more complicated than outlined in Sec. II.C, because it is necessary to account for the Mn-Mn interaction, the Fe-Fe interaction, as well as the Mn-Fe interaction. Moreover, it is necessary to take the Fe^{2+} fine structure

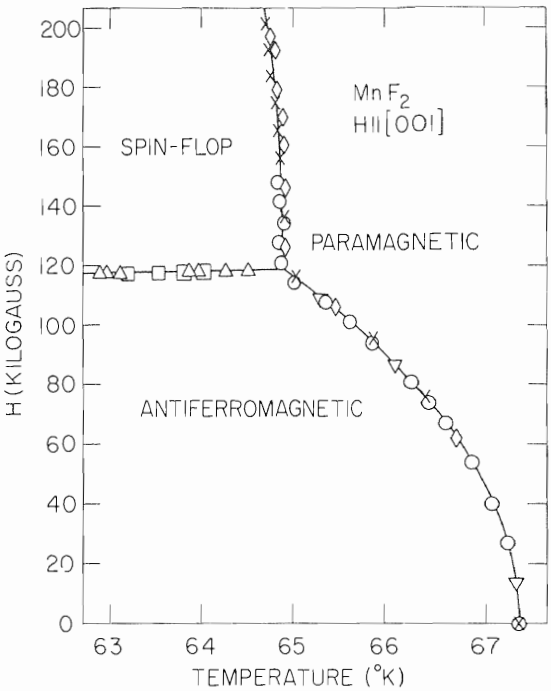

Fig. 7. Phase diagram of MnF_2, $H \parallel [001]$, close to T_N (after Ref. 2).

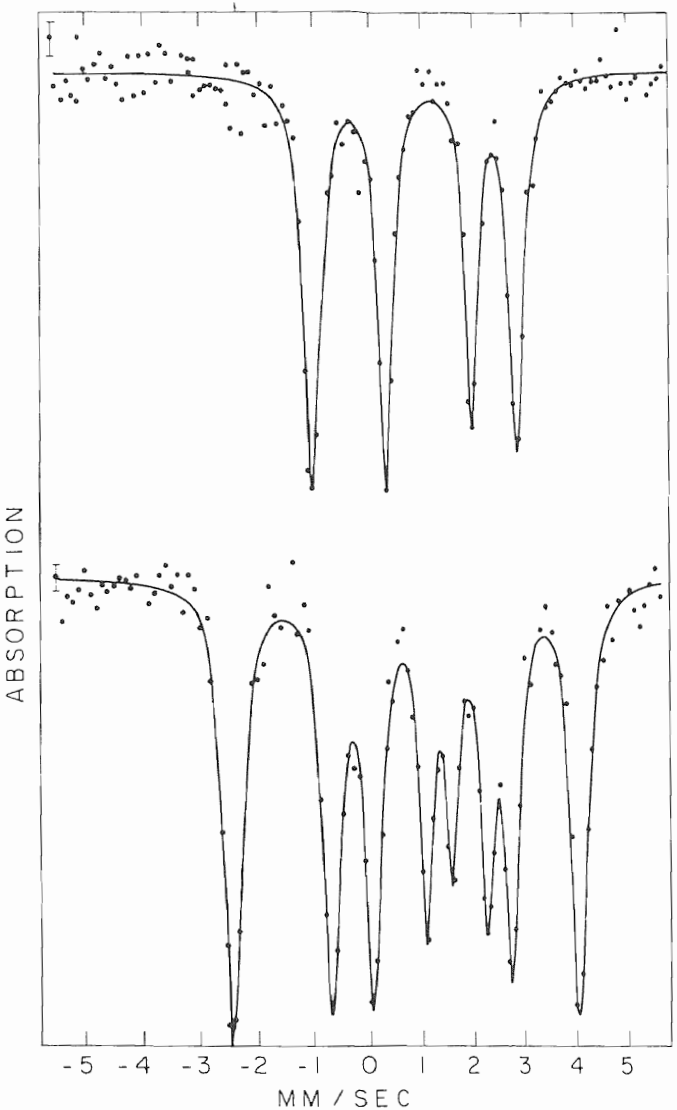

Fig. 8. Spectra of single crystal MnF_2:Fe^{2+} at 80 kOe parallel to [001] above (top spectrum) and below (bottom spectrum) T_N (after Ref. 9).

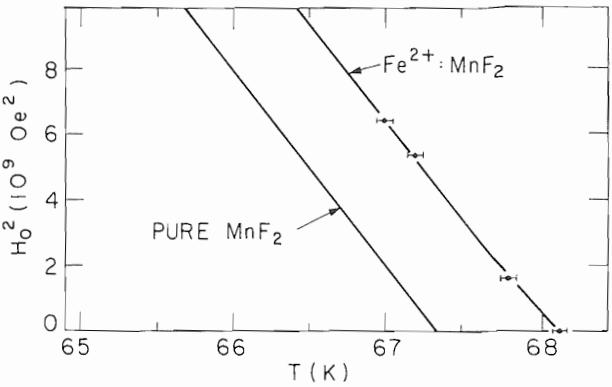

Fig. 9. H_o^2 at the AF-P phase boundary plotted as a function of T for MnF_2 and MnF_2:Fe^{2+} ($H_o \| [001]$) (after Ref. 9).

splitting into account. In the calculations shown in Fig. 10, J(Mn-Mn) and J(Fe-Fe) were taken from the Néel temperatures of pure MnF_2 and FeF_2 respectively, using the relation

$$J = \frac{3\,k\,T_N}{2zS\,(S+1)}$$

where z is the number of nearest neighbors. This reduces the number of parameters in the MFA to two, i.e., J(Mn-Fe) and the Fe^{2+} fine structure splitting. The latter can be obtained from the shift of H_{SF} with concentration in $Mn_xFe_{1-x}F_2$ crystals.[7] The value of the Mn-Fe exchange obtained,[9]

$$J(\text{Mn-Fe}) = -1.7\ \text{cm}^{-1},$$

is in fair agreement with determinations by other methods.

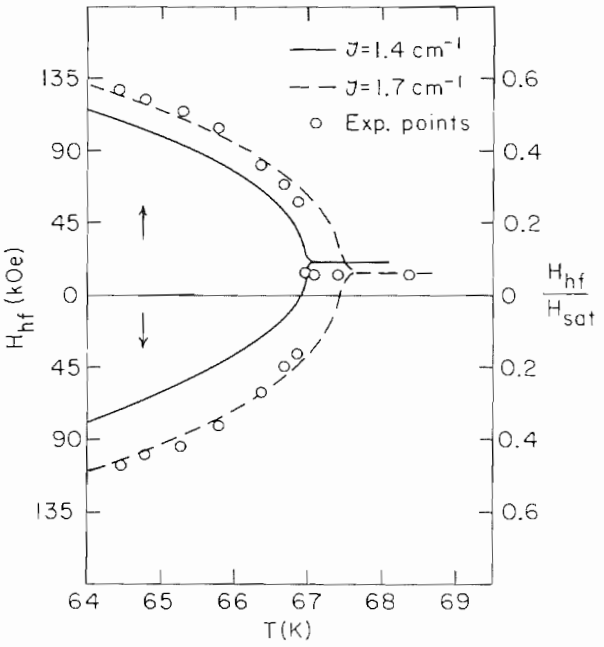

Fig. 10. $|H_{hf}|$ and $\sigma = H_{hf}/H_{sat}$ plotted as a function of T for H_o = 80 kOe, $H_o \parallel [001]$. The solid line is the best fit with the MFA, above and below T_N. The dashed line gives the best fit to the Néel temperature.

Critical Region. As explained in Sec. II, the best fit with the MFA breaks down near T_N. In Fig. 11 we show log L plotted as a function of log $(1 - T/T_N)$. Data for H_o = 0 and 80 kOe are shown plotted together with data obtained at H = 0 by Wertheim et al.[6] As can be seen, the same critical exponent $\beta = 0.334$ fits the data over the wide range of magnetic field, from 0 to 80 kOe.

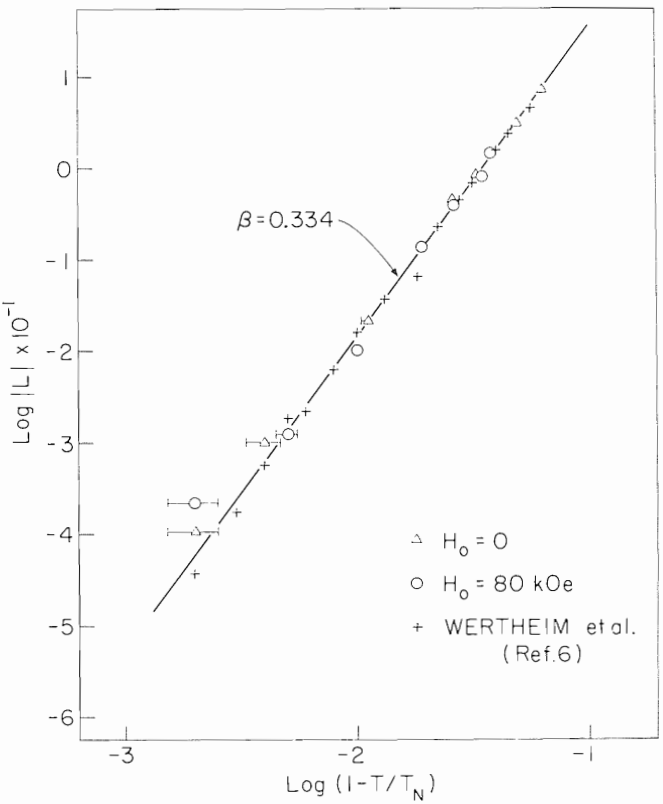

Fig. 11. Log L plotted as a function of Log $|T - T_N|$, for H_o = 0 and 80 kOe, with $H_o \parallel [001]$.

B. α-Fe_2O_3

Hematite (α-Fe_2O_3) is essentially antiferromagnetic below the Néel temperature $T_N \approx 960$ K.[10, 11] The magnetic structure is more complicated than the simple uniaxial antiferromagnet because the anisotropy, while small, is temperature dependent and in fact changes sign, leading to a spontaneous spin flip in zero magnetic field known as the Morin transition, with $T_m \approx 260$ K. For $T < T_m$, the spins are aligned antiparallel along the trigonal axis. For $T_m < T < T_N$, the spins lie in the basal plane, and are slightly canted toward each other. This canting is the source of the "weak ferromagnetism" in hematite above T_N. The Morin transition is easily observed in single crystal spectra[12] by the sudden change in the intensity of the $\Delta m = 0$ lines at T_m, as shown in Fig. 12. It can also be observed in powder spectra because β changes from 0° to 90° at T_m.[13]

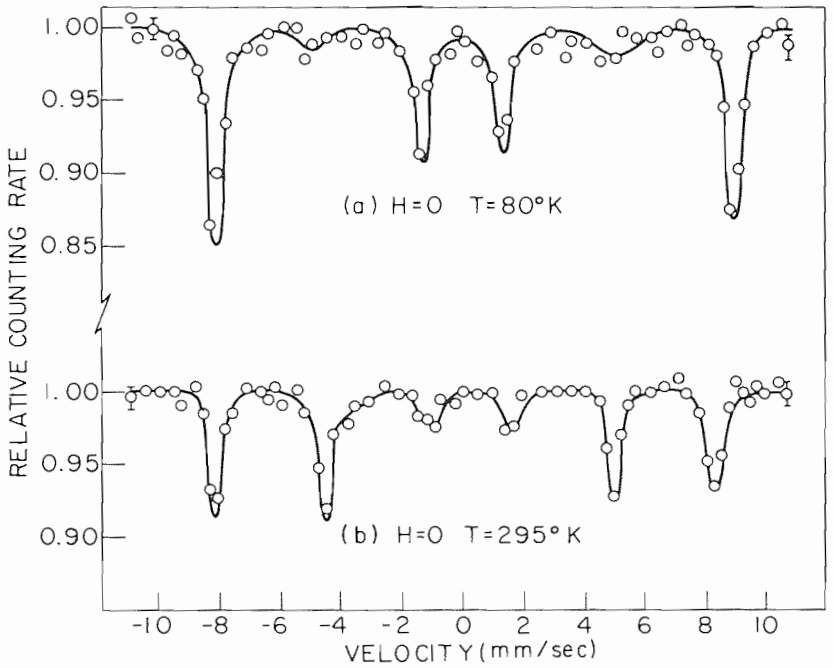

Fig. 12. Mössbauer spectra of single crystal α-Fe_2O_3 with $\gamma \parallel$ c-axis, above and below T_m (after Ref. 12).

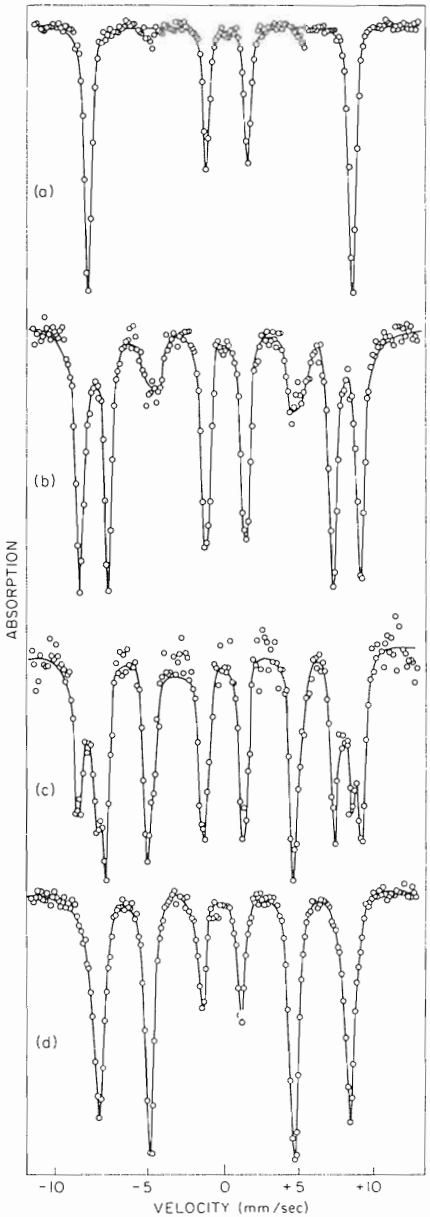

Fig. 13. Spectra of single crystal α-Fe_2O_3 at 4.2 K with $H_o \parallel c$: a) $H_o = 0$; b) $H_o = 65$ kOe; c) $H_o = 66.5$ kOe; d) $H_o = 70$ kOe.

H_o || Trigonal Axis. For $T < T_m$, a magnetic field applied parallel to the trigonal axis induces a first-order spin flop into the basal plane.[12] This is beautifully illustrated by the single crystal Mössbauer spectra in Fig. 13. At the spin flop, the intensity of the $\Delta m = 0$ lines changes as does β. Close examination of the spectra show that portions have flopped while other portions have not yet flopped; this is most easily seen in the structure of the outer lines. These "domains" could result from local variations in the anisotropy due to impurities or to local strains, perhaps introduced in producing a thin single crystal slice. The AF-SF phase boundary, determined by magnetic moment and ultrasonic attenuation measurements[14] is shown in Fig. 14. The transition fields at three temperatures determined by the Mössbauer effect[12, 15] are indicated in the figure, and are in good agreement with the determinations by the other methods.

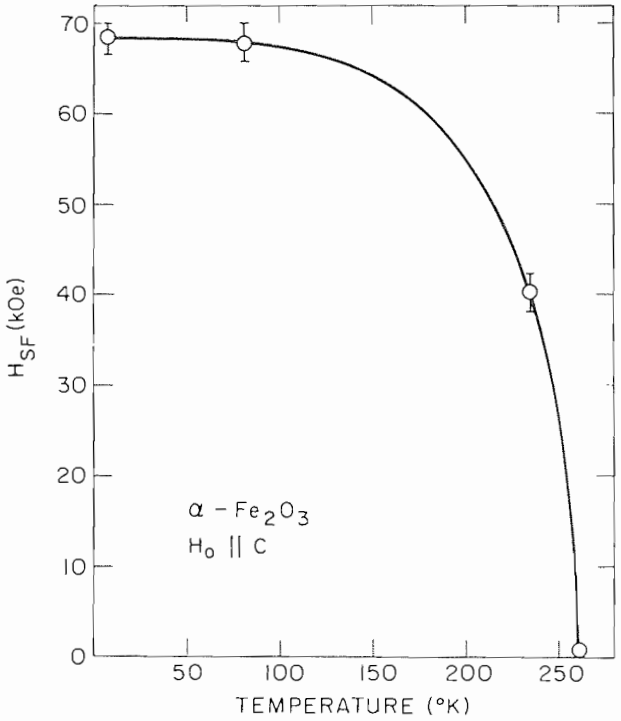

Fig. 14. Phase boundary of α-Fe_2O_3 (after Ref. 14). The data points are spin-flop fields determined by the Mössbauer spectra.

$H_o \perp$ Trigonal Axis. Because of the complicated anisotropy, H_o applied perpendicular to the trigonal axis will also induce a first-order spin flop.[14] This was studied close to T_m by Simkin and Bernheim[16] using the Mössbauer effect, and at lower temperature by Blum and Frankel.[15] The complete phase boundary was determined by ultrasonic and magnetic moment measurements.[14] Blum and Frankel[15] found from measurements of the intensity of the $\Delta m = 0$ lines as a function of H_o, that except close to T_m, the spins rotate away from the trigonal axis toward the basal plane before flopping. The rotation is large enough that the first-order transition could not be observed with the Mössbauer effect, except just below T_N.[15]

C. Metamagnetic Transitions and Complex Structures

$FeCl_2 \cdot 2H_2O$. Monoclinic $FeCl_2 \cdot 2H_2O$ orders antiferromagnetically at $T_N \approx 23$ K and the magnetic structure consists of two sublattices of $-FeCl_2-$chains lying along the c-axis.[17] The coupling along the chains is ferromagnetic with weak antiferromagnetic coupling between chains. Application of an external magnetic field along the easy axis a induces phase transitions at $H_1 = 39$ kOe and $H_2 = 46$ kOe.[17, 18]

Mössbauer studies of $FeCl_2 \cdot 2H_2O$ include a powder study by Chandra and Hoy[19] and a single crystal study by Johnson.[20] They found a magnetic hyperfine field of 250 kOe and an electric quadrupole interaction of 2.30 mm/sec with asymmetry parameter $\eta = 0.3$. The principle component of the efg is at right angles to the magnetic hyperfine field. Johnson[20] also determined that the spins lay in the ac plane at an angle of 66.2° from a axis, in agreement with results obtained by Narath[17] from susceptibility and proton magnetic resonance measurements.

Kandel et al.[21] have studied the magnetic phases at 4.2 in external fields. A single crystal, grown from solution, was oriented and cut so that the γ-ray propagation direction and H_o were parallel to the easy axis a. The spectra in various fields are shown in Fig. 15a, 15b, 15c and 15d. At $H_o = 0$ a four line spectrum is obtained, with a small absorption due to non-magnetic $FeCl_2 \cdot 4H_2O$. For $H_o < H_1$ the spectrum (Fig. 15b) consists of two superposed spectra of equal intensity corresponding to the external field H_o adding and subtracting respectively from the hyperfine fields for the ions in the spin down and spin up sublattice, respectively. For $H_1 < H_o < H_2$, the spectrum (Fig. 15c) consists of two super-

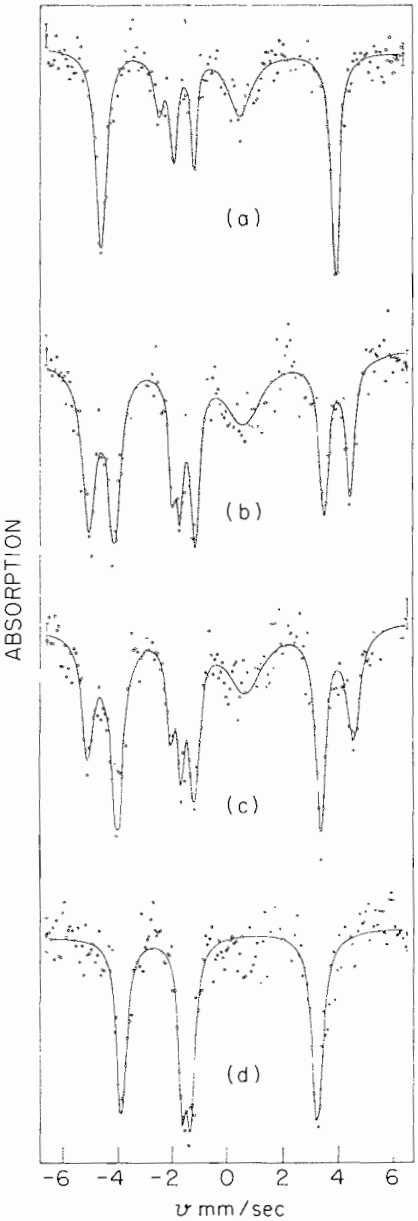

Fig. 15. Mössbauer spectra of $FeCl_2 \cdot 2H_2O$ at 4.2 K: a) $H_o = 0$, b) $H_o = 35$ kOe; c) $H_o = 42$ kOe; d) $H_o = 50$ kOe. In all cases $\gamma \parallel H_o \parallel$ easy axis (after Ref. 21).

posed spectra corresponding to the spin up and spin down sublattices, but now with relative intensities approximately 2:1. Since the majority spins have a smaller splitting than the minority spins, the sign of the hyperfine field is negative. For $H_2 < H_o$, a single spectrum is obtained (Fig. 15d). For all three phases, the sign magnitude and orientation of the efg is the same as in zero magnetic field, showing that the spins remain collinear in all three phases and that there is no spin canting. Moreover, the magnetic hyperfine interaction (exclusive of the applied field) is the same for all three phases (Fig. 16) indicating that the moment per ion is unchanged by increasing magnetic field or phase transitions.

The transition at 39 kOe is thus an AF to ferrimagnetic transition in which two spins are up and one spin down. The transition at H_2 = 46 kOe is a ferrimagnetic to P transition with all spins parallel. These results thus confirm the model proposed by Narath.[17]

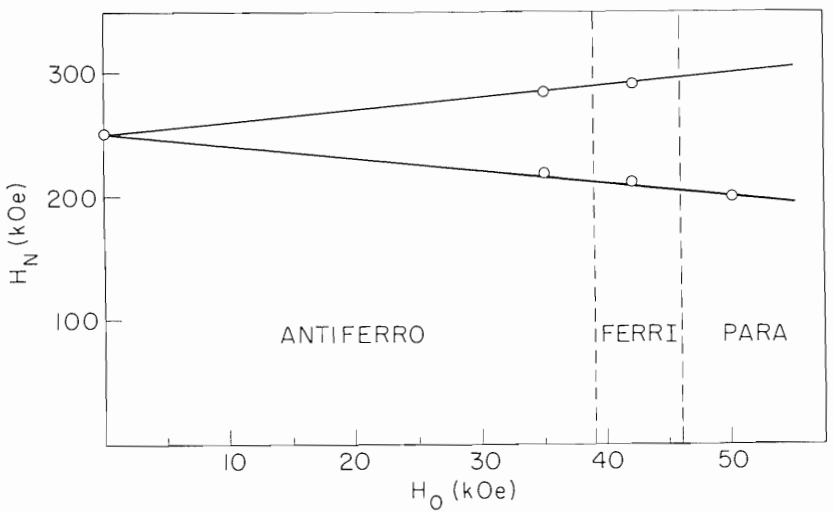

Fig. 16. H_n plotted as a function of H_o for the three phases of $FeCl_2 \cdot 2H_2O$ as determined from the spectra in Fig. 15.

$\underline{FeCl_2}$ and $\underline{FeBr_2}$. Simkin[22] has reported the Mössbauer spectroscopy of the metamagnetic transition in $FeCl_2$ and $FeBr_2$. In both cases, the spins are aligned antiferromagnetically along a threefold axis below the respective Néel temperatures (24 K for $FeCl_2$ and 11 K for $FeBr_2$). A metamagnetic transition is induced by an external magnetic field applied parallel to the threefold axis, at 10.5 kOe for $FeCl_2$ and 31.5 kOe for $FeBr_2$. In $FeCl_2$, the magnitude of the hyperfine field and the transition field are so low that the two sublattices cannot be resolved. In $FeBr_2$ marked changes in the $FeBr_2$ spectrum were observed on passage through the metamagnetic transition. The hyperfine field in $FeBr_2$ was found to be of positive sign (see Fig. 17) and a small change was observed in H_{hf} in going across the phase boundary. This change was shown by Simkin to be a change in the interionic dipole field in going from the AF to the P phase.

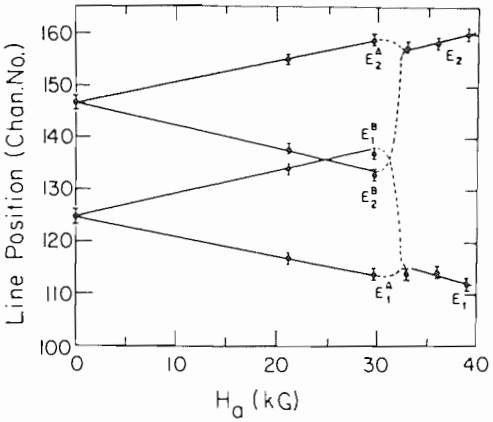

Fig. 17. Line position as a function of H_o for single crystal $FeBr_2$, with $H_o \parallel$ easy axis. At the transition field the two sublattices become co-parallel (after Ref. 22).

$\underline{FeCO_3}$. Forester and Koon[23] have made measurements in single crystals of $FeCO_3$. In this material the spins in the AF phase align antiparallel along the trigonal axis, below $T_N = 38$ K. An applied field $H_o \approx 200$ kOe is necessary to induce the metamagnetic transition. As Forester and Koon applied fields up to 120 kOe their measurements concerned

the AF phase. They observed that the spectral lines for one sublattice broadened with increasing T in a field H_o = 100 kOe, while the other did not. They argued that the sublattice with spins antiparallel to H_o will have a higher relaxation frequency because those spins are more easily flipped in an external field. A higher relaxation frequency means a greater line width at a given temperature. They were thus able to determine that the sign of the hyperfine field in $FeCO_3$ is positive.

$FeCl_3$. Anhydrous $FeCl_3$ has been thoroughly studied by Stampfel et al.[24] The Fe^{3+} are located in the interstices of a hexagonal close-packed lattice of Cl ions, and below T_N = 8.7 K, the spins order with a complex spiral-spin structure. Just below T_N, the lines are broad, indicating spin relaxation effects. Measurements of H_{hf} versus T fitted to Eq. (11) suggest that the dimensionality of ordering is two (β = 0.156), but neutron measurements show three dimensional order. Magnetic fields parallel to the c-axis induce phase transitions. In fields H_o < 15 kOe, a distribution of magnetic fields at the nuclei is observed as expected from the spiral magnetic structure at H_o = 0 determined by neutron diffraction. For 15 < H_o < 40 kOe, a two sublattice model satisfactorily accountes for the spectra. At H_o = 40 kOe, the spins changed orientation and the intensity of the $\Delta m = 0$ lines increased suddenly indicating a transition to an SF-like phase. The entire AF-SF phase boundary was determined and H_{SF} was found to increase slightly with increasing temperature, up to the intersection with the AF-P phase boundary. The possibility of a tri-critical point in the $FeCl_3$ phase diagram is also discussed as an explanation for the anomalously small value of β.

$FeCl_3 \cdot 6H_2O$. Carroll and Kaplan[25] have observed the AF to P transition in magnetic fields in $FeCl_3 \cdot 6H_2O$, which is antiferromagnetic below the Néel temperature T_N = 1.46 K. In their experiment they held the temperature constant at 1.16 K and increased the magnetic field, and obtained the spectra shown in Fig. 18, which beautifully illustrates the AF to P transition in this material at $H_{AFP} \approx 10$ kOe. The results can be understood in terms of the MFA and Fig. 3. For $0 < H_o < H_{AFP}$, there are two superposed spectra corresponding to spin up and spin down, with different field dependences of the hyperfine field H_{hf} apart from the simple subtraction and addition of H_o to H_{hf} on the respective spin up and spin down sublattices. For $H_o > H_{AFP}$, there is a single spectrum in which H_{hf} varies roughly as Eq. (15). For fields up to 20 kOe applied perpendicular to the spin axis they ob-

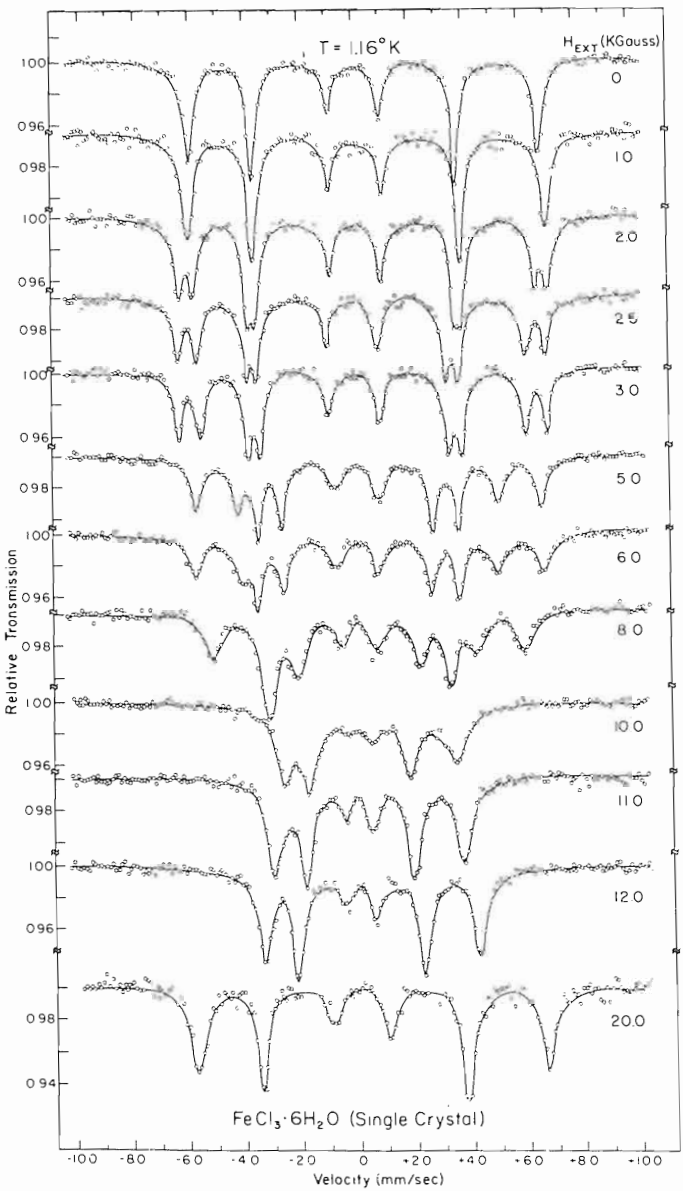

Fig. 18. Mössbauer spectra of single crystal $FeCl_3 \cdot 6H_2O$ at 1.16 K, $\gamma \perp H_o$. For the particular field direction, the AF to P transition occurs $8 < H_o < 10$ kOe.

served no transition. This is explicable in terms of the MFA because the AF to P transition with $H_o \perp a$ takes place at higher fields than for $H_o \parallel a$ (Eq. (9)). This is well illustrated experimentally by Shapira's ultrasonic attenuation study of the AF-P phase boundaries in FeF_2.[26]

V. CONCLUSION

We hope we have demonstrated that Mössbauer spectroscopy can be a very fruitful technique for studying magnetic field induced phases and phase changes in antiferromagnets. Of course, one needs external magnetic fields and single crystals, but the former are becoming increasingly available in the form of superconducting magnets and the latter can often be obtained if there is interest (and money). The study of the sublattice magnetization crossing the AF-P phase boundary can be made in any antiferromagnet containing iron and other Mössbauer nuclei and could prove interesting in the case of, for example, lower dimensional structures.

ACKNOWLEDGEMENTS

The participation of N. A. Blum, C. R. Abeledo, M. Weber, A. Misetich and L. Kandel in many of the experiments reported here is gratefully acknowledged. Y. Shapira, S. Foner and B. B. Schwartz provided useful and stimulating discussions and insights. We also thank Grace M. Lynch for her editorial assistance.

REFERENCES

+ Supported by the National Science Foundation.

1. S. Foner in Magnetism, Vol. I, edited by G. Rado and H. Suhl, Academic Press, New York, 1963, p. 383.
2. Y. Shapira and S. Foner, Phys. Rev. B1, 3083 (1970).
3. F. Keffer, Handbuch der Physik, Vol. 18-2, Springer Verlag, Berlin. 1966.
4. P. Heller, Phys. Rev. 146, 403 (1966).
5. Y. Shapira, J. Appl. Phys. 42, 1588 (1971).

6. G.K. Wertheim, H.J. Guggenheim and D.N.E. Buchanan Phys. Rev. Lett. 20, 1158 (1968); J. Chem. Phys. 51, 1931 (1969).

7. M.A. Lowe, A. Misetich and C.R. Abeledo, J. Phys. (Paris) 32, 1068 (1971).

8. C.R. Abeledo, R.B. Frankel, A. Misetich and N.A. Blum, J. Appl. Phys. 42, 1723 (1971).

9. C.R. Abeledo, R.B. Frankel, M.A. Weber and A. Misetich, AIP Conference Proceeding 10, 1168 (1973). A more complete version is being prepared for publication in the Physical Review.

10. I.S. Jacobs, R.A. Beyerlein, S. Foner and J.P. Remeika, Int. J. Mag. 1, 197 (1971).

11. Y. Shapira, Phys. Rev. 184, 589 (1969).

12. N. Blum, A.J. Freeman, J.W. Shaner and L. Grodzins, J. Appl. Phys. 36, 1169 (1965).

13. F. van der Woude, Phys. Status Solidi 17, 417 (1966).

14. S. Foner and Y. Shapira, Phys. Lett. A29, 276 (1969).

15. N. A. Blum and R.B. Frankel, Bull. Am. Phys. Soc. 12, 23 (1967) and unpublished data.

16. D.J. Simkin and R.A. Bernheim, Phys. Rev. 153, 621 (1967).

17. A. Narath, Phys. Rev. A139, 122 (1965).

18. M.A. Lowe, C.R. Abeledo and A. Misetich, AIP Conference Proceeding 5, 307 (1972).

19. S. Chandra and G.R. Hoy, Phys. Lett. 22, 254 (1966).

20. C.E. Johnson, Proc. Phys. Soc. Lond. 88, 943 (1966).

21. L. Kandel, M.A. Weber, R.B. Frankel and C.R. Abeledo, Phys. Lett. (to be published).

22. D.J. Simkin, Phys. Rev. 177, 1008 (1969).

23. D.W. Forester and N.C. Koon, J. Appl. Phys. 40, 1316 (1969).

24. J. P. Stampfel, W.T. Oosterhuis, B. Window and F. deS. Barros, Phys. Rev. B8, 4371 (1973).

25. T.X. Carroll and M. Kaplan, Chem. Phys. Lett. 22, 564 (1973).

26. Y. Shapira, Phys. Rev. B2, 2725 (1970).